International Journal of Pharmaceutics 434 (2012) 49–58

Contents lists available at SciVerse ScienceDirect

International Journal of Pharmaceutics

journal homepage: www.elsevier.com/locate/ijpharm

Pharmaceutical Nanotechnology

Dry powder inhaler formulation of lipid–polymer hybrid nanoparticles via electrostatically-driven nanoparticle assembly onto microscale carrier particles

Yue Yang[1], Wean Sin Cheow[1], Kunn Hadinoto*

School of Chemical and Biomedical Engineering, Nanyang Technological University, Singapore 637459, Singapore

ARTICLE INFO

Article history:
Received 28 March 2012
Received in revised form 30 April 2012
Accepted 17 May 2012
Available online 24 May 2012

Key words:
Chitosan
Dextran sulphate
Hybrid nanoparticles
Pulmonary delivery
Lipids
Adsorption

ABSTRACT

Lipid–polymer hybrid nanoparticles have emerged as promising nanoscale carriers of therapeutics as they combine the attractive characteristics of liposomes and polymers. Herein we develop dry powder inhaler (DPI) formulation of hybrid nanoparticles composed of poly(lactic-co-glycolic acid) and soybean lecithin as the polymer and lipid constituents, respectively. The hybrid nanoparticles are transformed into inhalable microscale nanocomposite structures by a novel technique based on electrostatically-driven adsorption of nanoparticles onto polysaccharide carrier particles, which eliminates the drawbacks of conventional techniques based on controlled drying (e.g. nanoparticle-specific formulation, low yield). First, we engineer polysaccharide carrier particles made up of chitosan cross-linked with tripolyphosphate and dextran sulphate to exhibit the desired aerosolization characteristics and physical robustness. Second, we investigate the effects of nanoparticle to carrier mass ratio and salt inclusion on the adsorption efficiency, in terms of the nanoparticle loading and yield, from which the optimal formulation is determined. Desorption of the nanoparticles from the carrier particles in phosphate buffer saline is also examined. Lastly, we characterize aerosolization efficiency of the nanocomposite product in vitro, where the emitted dose and respirable fraction are found to be comparable to the values of conventional DPI formulations.

1. Introduction

Inhaled delivery of therapeutic nanoparticles has been extensively investigated in recent years motivated by the bioavailability enhancement potential afforded by the nanoparticles as they can effectively evade the phagocytic and mucociliary clearance mechanisms of the lung (Sung et al., 2007). Lipid–polymer hybrid nanoparticles, where polymer nanoparticle core is enveloped by lipid layers, represent a new generation of nanoscale therapeutic carriers, which combine the superior characteristics of polymer nanoparticles (i.e. structural integrity, controlled release capability) and liposomes (i.e. cell affinity and cell targeting ability) (Zhang et al., 2008). Moreover, hybrid nanoparticles in general exhibit higher hydrophobicity than polymer nanoparticles resulting in enhanced cell uptake and lower cytotoxicity (Su et al., 2011).

To successfully deliver hybrid nanoparticles, in fact any nanoparticles, by inhalation, they first have to be transformed into microscale nanocomposite structures having theoretical aerodynamic diameter ($d_{A,theory}$ in Eq. (1)) between 1 and 5 μm (Edwards, 2002), where d_G and ρ_e are particle geometric diameter and effective density, respectively. In this regards, particles with $d_{A,theory} \ll 1$ μm are exhaled, while those with $d_{A,theory} \gg 5$ μm predominantly deposit in the mouth and throat regions, instead of the lung. For hybrid nanoparticles, dry powder inhaler (DPI) mode of delivery is preferred over inhaled aqueous suspension, used in nebulization or metered dose inhaler (MDI), because the dry powder form can better ensure shelf life stability of the lipid.

$$d_{A,theory} = d_G \sqrt{\frac{\rho_e}{1\ g/cm^3}} \quad (1)$$

Conventionally, DPI formulations of therapeutic nanoparticles are prepared by spray drying (SD) (Kho et al., 2010; Sung et al., 2009), spray freeze drying (SFD) (Schiffter et al., 2010), or electrostatically-driven flocculation of the nanoparticles (El-Gendy and Berkland, 2009; Shi et al., 2007). In our earlier work (Wang et al., 2012), we investigated the use of SD and SFD techniques

Abbreviations: AA, acetic acid; CS, chitosan; DCM, dichloromethane; DI, deionized; DPI, dry powder inhaler; DXT, dextran sulphate; ED, emitted dose; FE-SEM, field emission scanning electron microscope; FPF, fine particle fraction; IP, induction port; MDI, metered dose inhaler; MMAD, mass median aerodynamic diameter; MW, molecular weight; NGI, next generation impactor; PC, phosphatidylcholine; PCS, photon correlation spectroscopy; PLGA, poly(lactic-co-glycolic acid); PPVS, potassium polyvinyl sulphate; PS, pre-separator; PTS, protamine sulphate; PVA, polyvinyl alcohol; SA, stearylamine; SD, spray drying; SFD, spray freeze drying; TPP, sodium tripolyphosphate.

* Corresponding author. Tel.: +65 6514 8381; fax: +65 6794 7553.
E-mail address: kunnong@ntu.edu.sg (K. Hadinoto).

[1] [1]These authors contribute equally to this work.

0378-5173/$ – see front matter © 2012 Elsevier B.V. All rights reserved.
http://dx.doi.org/10.1016/j.ijpharm.2012.05.036

Nomenclature

d_A	aerodynamic particle diameter (μm)
$d_{G,dry}$	volume-averaged geometric particle diameter after drying (μm)
$d_{G,wet}$	volume-averaged geometric particle diameter before drying (μm)
$d_{A,theory}$	volume-averaged aerodynamic particle diameter from theory (μm)
$M_{Carrier\ initial}$	mass of carrier particles used in nanoparticle adsorption experiment (mg)
$M_{Nanoparticle\ adsorbed}$	mass of nanoparticles used in nanoparticle adsorption experiment (mg)
$M_{Product}$	mass of nanoparticle assembly produced (mg)
$M_{Nanoparticle\ adsorbed}$	mass of nanoparticles adsorbed onto carrier particles (mg)
% nanoparticle loading	mass percentage of nanoparticles in the total product mass
% nanoparticle recovery	mass percentage of adsorbed nanoparticles relative to the initial mass
$R_{Nanoparticle/carrier}$	mass ratio of nanoparticle to carrier particle supplied
ρ_e	particle effective density (g/cm^3)

to prepare DPI formulation of hybrid nanoparticles made up of poly(lactic-co-glycolic acid) (PLGA) nanoparticles enveloped by phosphatidylcholine (PC) layers from soybean lecithin. With the help of multiple drying adjuvants (e.g. PVA, leucine), spherical aggregates of the PLGA–PC hybrid nanoparticles having the desired aerosolization characteristics were successfully produced. The role of the drying adjuvant was to protect the physicochemical integrity of the nanoparticles upon their exposures to extreme temperatures of hot air (≥80 °C) and liquid N_2 (≤−200 °C) in SD and SFD, respectively. The drawbacks of SD and SFD are that painstaking formulations of the drying adjuvants (i.e. type, compositions) need to be carried out each time different nanoparticles are used.

Moreover, the production yield of SD was low for particles in this size range, where only ≈20% of the hybrid nanoparticles were recovered as products (Wang et al., 2012). A majority of the nanoparticles in SD were lost in the cyclone separator walls as the lipid transformation into its wax-like state at high temperatures made the particle sticky. For SFD, a higher yield was obtained provided that the loss of nanoparticles during atomization into liquid N_2 was minimized, which required the use of a liquid N_2 vessel with wide neck opening, hence a large amount of liquid N_2 (Wang et al., 2012). The extensive use of liquid N_2, however, poses several hazards (e.g. asphyxiation, pressure buildup, cold burns) and costly logistic issues, particularly upon scale up.

One technique that can produce microscale nanocomposite structures at high yield and with minimal hazards is by inducing nanoparticle flocculation via electrostatic interactions. This technique requires the preparation of oppositely-charged nanoparticles (Shi et al., 2007), or the use of flocculating agent (e.g. leucine) to disrupt colloidal stability of the nanoparticles (El-Gendy and Berkland, 2009). Despite their irregular shapes and wide size distributions, flocs with excellent aerosolization characteristics were successfully prepared (El-Gendy and Berkland, 2009; Shi et al., 2007). Whether flocs with similar physical characteristics (e.g. size, shape, porosity) can be consistently produced between batches and upon scale-up, however, remains questionable. Importantly, similar to the adjuvant formulations in SD and SFD, the optimal condition for flocculation is likely specific to one type of nanoparticles.

Herein we present a new approach to prepare DPI formulation of lipid–polymer hybrid nanoparticles that addresses the limitations of the SD, SFD, and electrostatic flocculation techniques. The new approach is based on electrostatically-driven assembly of the nanoparticles onto oppositely charged microscale spherical carrier particles. In contrast to SD and SFD, the electrostatically-driven nanoparticle assembly takes place in an ambient condition, which eliminates the need for intricate formulations to protect the nanoparticles. The ambient preparation condition also results in minimal safety risks and low operating costs upon scale up. Unlike the electrostatic flocculation, nanocomposite particles having consistent physical characteristics between batches can be produced using our new approach as the carrier particles function as fixed templates for the nanoparticle adsorption. Importantly, the new approach would be applicable to different hybrid nanoparticles, with minimal modifications, provided that the nanoparticles are oppositely charged to the carrier particles. In terms of the scalability of the nanoparticle adsorption process, it is anticipated to be straightforward as it involves only mixing of two aqueous suspension, where as long as the degree of mixing is maintained upon scale up, the same nanocomposite particle would be produced.

In our new approach, polysaccharide carrier particles having the desired aerosolization characteristics and physical robustness are first prepared, followed by nanoparticle adsorption onto the carrier particles. Chitosan, a natural biocompatible and biodegradable polysaccharide widely used for drug delivery (Agnihotri et al., 2004), is used as the carrier material. Adsorptions of both cationic and anionic PLGA/PC hybrid nanoparticles onto the chitosan carrier particles are investigated at different nanoparticle to carrier mass ratios. The adsorption efficiency is characterized in terms of the nanoparticle yield and loading. As the adsorption is driven by electrostatic interaction, the effects of salt inclusion on the adsorption efficiency and desorption of the nanoparticles from the carrier particles are examined. Lastly, aerosolization efficiency of the nanocomposite particles is characterized in vitro using a cascade impactor and the results are compared with those obtained from existing DPI formulations.

2. Materials

Chitosan (CS) (MW = 310 kDa, 80–2000 cP, degree of deacetylation > 75%), sodium tripolyphosphate (TPP), dextran sulphate (DXT) (MW = 5000 Da), soybean lecithin (PC), stearylamine (SA), acetic acid (AA), dichloromethane (DCM), sodium chloride (NaCl), Pluronic F68, phosphate buffer saline (PBS), protamine sulphate (PTS), o-toluidine blue, and fluorescence dyes – rhodamine 6G and calcein – are purchased from Sigma Aldrich (USA). PLGA 50:50 (Purasorb 5004A) is a gift from PURAC Biomaterials (Netherlands). Potassium polyvinyl sulphate (PPVS) is purchased from Wako Pure Chemicals (Japan).

3. Methods

3.1. Preparation and characterization of lipid–polymer hybrid nanoparticles

Anionic PLGA–PC and cationic PLGA–PC/SA nanoparticles prepared by emulsification-solvent-evaporation method are used as the hybrid nanoparticle models. To prepare the anionic nanoparticles, 30 mg PC and 90 mg PLGA are dissolved in 3 mL DCM and then poured into 12 mL deionized (DI) water under ultrasonication for 90 s. The resultant nanoparticle suspension is stirred overnight at room temperature to evaporate off the DCM. Afterwards, the suspension is centrifuged at 14 000 rpm for 20 min and washed thrice with DI water to remove excess PC. To prepare the cationic nanoparticles, 3 mg SA is added together with 90 mg PLGA and 27 mg PC into the 3 mL DCM solution. To quantify the nanoparticle adsorption,

fluorescent dye is incorporated into the PLGA–PC/SA nanoparticles by adding 15 mg rhodamine in the DCM solution. For the PLGA–PC nanoparticles, 4.3 mg calcein dye is dissolved in 300 μL DI water then added to the DCM solution. The nanoparticle size and zeta potential are measured by photon correlation spectroscopy (PCS) using a Brookhaven 90Plus Nanoparticle Size Analyzer (Brookhaven Instruments Corporation, USA).

3.2. Preparation and characterization of polysaccharide carrier particles

3.2.1. Preparation of CS/TPP/DXT particles by ionic crosslinking

The polysaccharide carrier particles are prepared by ionic crosslinking of CS with TPP and DXT using a two-fluid atomizer (BÜCHI B-290, Switzerland). CS is dissolved in 10 mL of 1.0% (v/v) aqueous AA solution. The 1.0% (w/v) CS solution is atomized into 500 mL aqueous TPP solution at a certain TPP to CS concentration ratio in 3 L beaker under constant stirring. The CS solution feed rate and atomization flow rate are fixed at 14 mL/h and 1370 L/h, respectively. The large beaker is used to maximize the production yield by preventing the atomized CS solution from hitting the container walls. Up to 80% (w/w) CS yield is achieved as a result. The distance between the atomizer nozzle and the solution is kept at 40 cm. pH of the TPP solution is adjusted to 5.0 with AA to optimize the crosslinking density, hence structural integrity of the carrier particles (Bhumkar and Pokharkar, 2006). For the size range investigated in the present work, 0.2% (v/v) Pluronic F68 must be added into the TPP solution to minimize agglomeration of the crosslinked particles on the liquid-air interface. The crosslinked particles are aged in the solution for 1 h after which the suspension is washed thrice by centrifugation at 4000 rpm for 10 min and rinsing with DI water. TPP solution is filtered and reused for the next batch of experiment. When DXT is used as an additional crosslinker, DXT is added into the TPP solution.

The CS/TPP crosslinking is carried out at excess TPP to CS charge ratio to obtain nearly 100% crosslinking of CS. The charge ratio is determined from charge density calculations involving MW and the number of charge per molecule. The MWs are 155 g/mol per monosaccharide of CS, 368 and 5000 g/mol for TPP and DXT, respectively. The numbers of charge per molecule are 0.73 per monosaccharide of CS, 5 for TPP, and 24 for DXT. The resultant charge densities are 4.7×10^{-6}, 1.36×10^{-5}, and 4.8×10^{-6} mol-charge/mg for CS, TPP, and DXT, respectively. Equal concentrations of CS and TPP therefore translate to excess TPP charge at around three times of the CS charge.

3.2.2. Physical characterizations

The geometric particle size in the aqueous suspension state ($d_{G,wet}$) is determined by analyzing the light microscope images (Olympus CKX41, Japan) with minimum of 200 particle counts. Colloidal titration, based on stoichiometric interactions between positive and negatively charged colloidal particles, is performed to determine charge density of the wet carrier particles (Kam and Gregory, 1999). The charge density is characterized in the wet state in which the nanoparticle adsorption takes place. The step-by-step procedures of the charge titration are presented in the Supplementary Information. The dry-powder form is prepared by overnight freeze drying of the aqueous suspension. The geometric particle size after drying ($d_{G,dry}$) is determined by image analysis using field emission scanning electron microscope (FE-SEM) (JSM-6700F, JEOL, USA) with minimum of 400 particle counts. ρ_e is determined from tap density after 2000 taps using tap densitometer (Quantachromme, USA). Experimental uncertainties in the $d_{G,dry}$ and ρ_e measurements are 7% and 3–8%, respectively, based on minimum of three replicates. $d_{A,theory}$ is calculated using Eq. (1) from the experimental values of $d_{G,dry}$ and ρ_e.

3.3. Nanoparticle adsorption and desorption

200 μL of the nanoparticle suspension at varying mass concentrations ($M_{Nanoparticle\ initial}$) are added to 300 μL of the carrier particle suspension containing 10 mg particles ($M_{Carrier\ initial}$) under gentle stirring. The mixture is then put in a shaking incubator for 30 min at 250 rpm for the nanoparticle adsorption to take place. The resultant nanocomposite particles (i.e. product) undergo three cycles of centrifugation at 3000 rpm for 3 min and washing with DI water to remove the non-adsorbed nanoparticles. The washed product is weighted after freeze drying ($M_{Product}$) to determine the % nanoparticle recovery and % nanoparticle loading, which are defined in Eqs. (2) and (3), respectively. The values reported are based on a minimum of three replicates. The effects of $R_{Nanoparticle/carrier}$, which is defined as $M_{Nanoparticle\ initial}/M_{Carrier\ initial}$, on the % recovery and % loading are investigated at $0.26 \le R_{Nanoparticle/carrier} \le 1.68$. The effects of salt inclusion are examined using 0.1 M aqueous NaCl solution.

$$\%\ \text{nanoparticle recovery} = \frac{M_{Nanoparticle\ adsorbed}}{M_{Nanoparticle\ initial}} \times 100\% = \frac{M_{Product} - M_{Carrier\ initial}}{M_{Nanoparticle\ initial}} \times 100\% \quad (2)$$

$$\%\ \text{nanoparticle loading} = \frac{M_{Nanoparticle\ adsorbed}}{M_{Product}} \times 100\% \quad (3)$$

The % recovery and % loading obtained by the mass measurements are verified by UV–Vis spectroscopy analysis of the fluorescent dye in the nanoparticles. Briefly, a known mass of the product is put into 1 mL DCM to dissolve the nanoparticles after which it is centrifuged at 14,000 rpm. Rhodamine and calcein concentrations in the supernatant are measured at 521 and 485 nm, respectively. From the known fluorescence loading in the nanoparticles (≈2.0%, w/w), the amount of nanoparticle adsorbed is determined and is used to calculate the % nanoparticle loading and recovery. The nanoparticle adsorption is verified visually using FE-SEM and fluorescence microscope (Axio Scope A1, Carl Zeiss, Germany).

To assess the nanoparticle desorption, 0.5 mL of the product suspension, which contains about 2.5 mg of nanoparticles, is placed in 25 mL PBS solution at 37 °C and left for 2 h in a shaking incubator. Afterwards, the suspension is centrifuged at 6000 rpm for 10 min and the sediment is washed thrice. The mass of sediments is measured to determine the particle mass loss due to nanoparticle desorption. The desorption experiment is carried out in triplicates. A similar procedure is followed for the dry product using 7 mg of sample.

3.4. Aerosolization efficiency characterizations

$d_{G,dry}$, ρ_e, and $d_{A,theory}$ of the nanocomposite particles are determined by the same methods detailed in Section 3.2.2. The aerosolization efficiency is characterized in terms of three parameters i.e. emitted dose (ED), fine particle fraction (FPF), and mass median aerodynamic diameter (MMAD). A seven-stage Next Generation Impactor (NGI) (Copley Scientific, UK) equipped with an induction port (IP) and a pre-separator (PS) is used. A powder dispatchment tube (PDT) is used in place of an inhaler to enable characterization of the aerosolization efficiency independent of the inhaler type (Wang et al., 2012). ED is defined as the mass percentage of the particles that is successfully entrained off the PDT, FPF is defined as the mass percentage of the entrained particles having

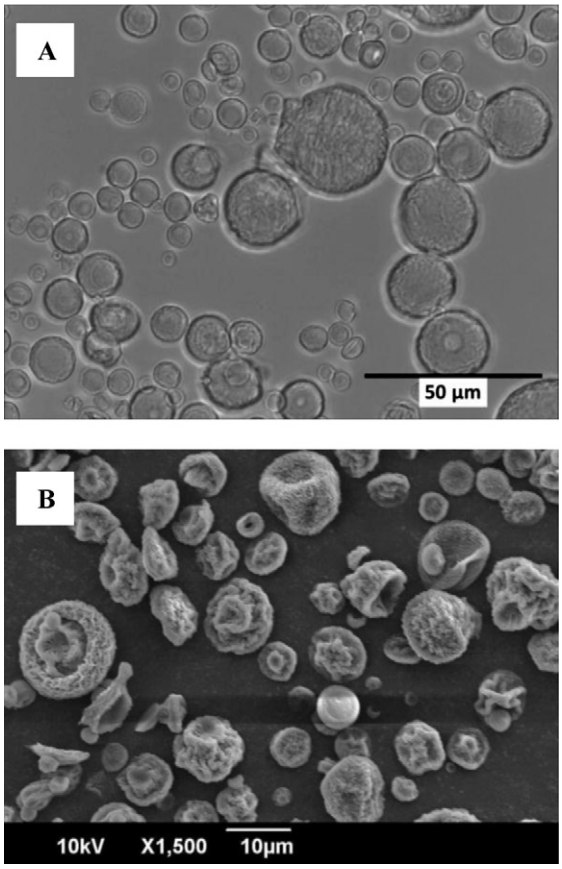

Fig. 1. CS/TPP/DXT blank carrier particles at CS:TPP:DXT = 1.0:1.0:1.0% (w/v) (A) before freeze drying under light microscope and (B) after freeze drying under FE-SEM.

d_A below 5 μm, and MMAD is the median d_A of the entrained particles based on mass. Briefly, 19 mg of product are aerosolized at 85 L/min to achieve the recommended 4 kPa pressure drop across the PDT. The airflow duration is fixed at 2.8 s to mimic 4 L of air drawn in human inhalation. The cut-off d_A at 85 L/min are 6.7, 3.7, 2.4, 1.4, 0.8, 0.5 and 0.3 μm for stages 1–7, respectively. The powders deposited in each stage are collected with DI water and freeze dried to determine the mass. Similar to the % loading and recovery, the results have been validated with UV–Vis analysis of the fluorescence dye. The reported ED, FPF, and MMAD are based on a minimum of two replicates.

4. Results

4.1. Inhalable carrier particles

A summary of the different experimental runs carried out to produce carrier particles, which possess $1 \leq d_{A,theory} \leq 5$ μm, is presented in Table 1. The starting point is at CS and TPP concentrations of 1.0% and 2.5% (w/v), respectively, which produces well dispersed CS/TPP particles with $d_{G,wet} \approx 10$–30 μm. The CS/TPP particles, however, severely aggregate after freeze drying as shown in Fig. S1 of the Supplementary Information, rendering them non aerosolizable. Their dry-powder characteristics (i.e. $d_{G,dry}$ and ρ_e) are thus not reported in Table 1. DXT is added into the CS/TPP formulation in Run 2 at 1.0: 1.0: 1.0% (w/v) concentrations. The light microscope image in Fig. 1A shows that the wet CS/TP/DXT particles are well dispersed with $d_{G,wet} \approx 10$–30 μm, hence they are fairly similar to the CS/TPP particles produced in Run 1. Importantly, the particles remain dispersed after freeze drying (Fig. 1B) with

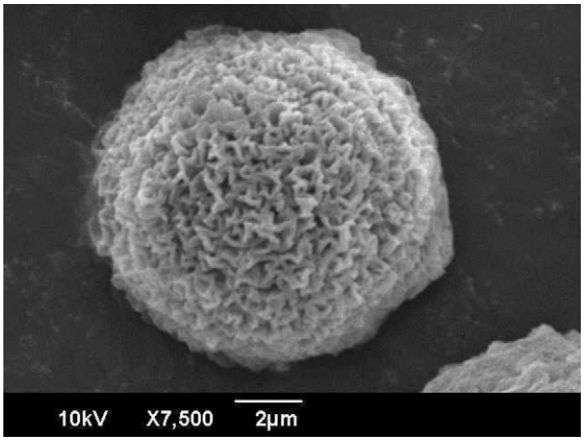

Fig. 2. The highly corrugated surface of the CS/TPP/DXT particles.

$d_{G,dry} \approx 6.4$ μm and $\rho_e = 0.54$ g/cm^3 resulting in $d_{A,theory} \approx 4.7$ μm signifying their suitability for DPI delivery. The considerably larger $d_{G,wet}$ compared to $d_{G,dry}$ is due to CS swelling in aqueous medium. A closer look at the freeze dried particles in Fig. 2 indicates a highly corrugated surface, not observed in CS/TPP particles, suggesting the likely presence of DXT on the particle surface.

As the nanoparticle adsorption is anticipated to increase ρ_e resulting in $d_{A,theory} \geq 5$ μm for the product, an attempt to lower $d_{A,theory}$ of the carrier particles is carried out in Run 3 by reducing both TPP and DXT concentrations to 0.5% (w/v). The lower crosslinker concentrations are thought to lower ρ_e due to reduced crosslinking. The results, however, indicate otherwise, where ρ_e is increased to 0.62 g/cm^3, which coupled with an increase in $d_{G,dry}$ to 7.4 μm results in $d_{A,theory} > 5$ μm. Another attempt to lower $d_{A,theory}$ of the carrier particles is by reducing the CS, TPP, and DXT concentrations to 0.5% (w/v). The particles produced are poorly dispersed, even in their wet state, as shown in Fig. S2 of the Supplementary Information.

The charge density of the CS/TPP/DXT particles in Run 2 is -1.9 ± 0.2 mequiv./g, which is considerably higher than that of the CS/TPP particles in Run 1 (-1.1 ± 0.2 mequiv./g) owed to the presence of anionic DXT on the surface. Importantly, the blank carrier particles exhibit ED = 75 ± 1% (w/w) and FPF = 27 ± 7% (w/w) resulting in MMAD = 4.9 ± 0.8 μm denoting their suitability for DPI delivery, consistent with their $d_{A,theory}$ of 4.7 μm.

4.2. Hybrid nanoparticle adsorption and desorption

The sizes of both the cationic PLGA–PC/SA and anionic PLGA–PC nanoparticles are ≈120–150 nm with zeta potentials of (+) 34 and (−) 33 mV, respectively. The cationic PLGA–PC/SA nanoparticles are readily adsorbed onto the oppositely charged CS/TPP/DXT carrier particles as shown in the fluorescence microscope images in Fig. 3A. In contrast, the anionic PLGA–PC nanoparticles are not adsorbed at all due to repulsive electrostatic forces from the highly negatively charged CS/TPP/DXT particles (Fig. 3B). These results confirm that the nanoparticle adsorption onto the carrier particles is electrostatically driven, and not due to other interaction mechanisms (e.g. hydrophobic). The FE-SEM images of the PLGA–PC/SA product in Fig. 4 show uniform coverage of the carrier particle surface by the nanoparticles, where the nanoparticles are uniformly dispersed, without noticeable segregation of the nanoparticles, on the carrier particle surface.

The effects of $R_{Nanoparticle/carrier}$ on the % nanoparticle recovery and loading of the PLGA–PC/SA nanoparticles are presented in Fig. 5. The % recovery is at the highest (≈85%) at the lowest $R_{Nanoparticle/carrier}$ investigated (i.e. 0.26), which denotes highly

Table 1
Effect of CS:TPP:DXT ratios on the carrier particle characteristics.

Run	CS (w/v)	TPP (w/v)	DXT (w/v)	Aggregate wet	$d_{G,wet}$ (μm)	Aggregate dry	$d_{G,dry}$ (μm)	ρ_e (g/cm^3)	$d_{A,theory}$ (μm)
1	1.0	2.5	0	No	20–30	Yes	–	–	–
2	1.0	1.0	1.0	No	10–30	No	6.4	0.54	4.7
3	1.0	0.5	0.5	No	10–30	No	7.4	0.62	5.8

effective adsorptions, whereby only 15% of the nanoparticles added is lost in the process. The % loading at this $R_{Nanoparticle/carrier}$, however, is only ≈18%, which is too low for an effective drug delivery. Increasing $R_{Nanoparticle/carrier}$ does lead to an increase in the % loading, though it reaches a plateau at ≈33% for $R_{Nanoparticle/carrier} \geq 0.83$ (Fig. 5A). The % recovery nevertheless continues to decrease with increasing $R_{Nanoparticle/carrier}$ indicating less efficient adsorptions at high $R_{Nanoparticle/carrier}$ (Fig. 5B). Therefore, the optimal $R_{Nanoparticle/carrier}$ is found in the region between 0.53 and 0.83, where both % recovery and % loading are at their reasonably high values. Taking into account the experimental uncertainties, the % recovery and % loading are basically constant at $0.53 \leq R_{Nanoparticle/carrier} \leq 0.83$ at ≈65% and 30%, respectively.

The salt inclusion has minimal impacts on the % loading and % recovery at both $R_{Nanoparticle/carrier}$ investigated, where the changes in the % loading and recovery fall within the experimental uncertainties. For both the wet and dry products, only ≈30 ± 3% (w/w) of the PLGA–PC/SA nanoparticles adsorbed onto the CS/TPP/DXT carrier particles are desorbed after 2 h exposure in PBS. Lastly, the % loading and % recovery obtained by mass measurements in Fig. 5 agree with those obtained from UV–Vis spectroscopy (Fig. 6).

4.3. Aerosolization efficiency of the nanocomposite particles

$d_{G,dry}$ and $d_{A,theory}$ of the nanocomposite particles produced at $0.53 \leq R_{Nanoparticle/carrier} \leq 0.83$ are presented in Fig. 7A. $d_{G,dry}$ varies from ≈7 μm at $R_{Nanoparticle/carrier} = 0.53$ and 0.75 to ≈9 μm at $R_{Nanoparticle/carrier} = 0.83$. At $R_{Nanoparticle/carrier} = 0.83$, the volume-based distribution of $d_{G,dry}$ constructed using a bin size of 5 μm in Fig. 7B denotes a monomodal distribution spanning between 5 and 25 μm. Similar size distributions are observed at $R_{Nanoparticle/carrier} = 0.53$ and 0.75 hence they are not presented here. The monomodal distribution of the nanocomposite particles is similar to that of the blank carrier particles, where the shift to larger $d_{G,dry}$ for the product is due to the nanoparticles adsorbed on the carrier particles. The span of the size distribution, however, is wider for the nanocomposite particles. The change in the $d_{G,dry}$ span width indicates that the extent of the nanoparticle adsorption is not uniform across the different carrier particle sizes. Owed to the similar % nanoparticle loading, the nanocomposite particles exhibit minimal variations in ρ_e as a function of $R_{Nanoparticle/carrier}$ with $\rho_e \approx 0.50 \pm 0.05$ g/cm^3. These combinations of $d_{G,dry}$ and ρ_e result in $d_{A,theory} \approx 5$–6 μm, which lies at or slightly above the desired $d_{A,theory}$.

ED, FPF, and MMAD of the nanocomposite particles produced at $R_{Nanoparticle/carrier} = 0.53$ and 0.83 are presented in Fig. 8. Aerosolization efficiency of the nanocomposite particles produced at $R_{Nanoparticle/carrier} = 0.75$ are not characterized as they possess similar $d_{G,dry}$ and $d_{A,theory}$ as those produced at $R_{Nanoparticle/carrier} = 0.53$.ED, FPF, and MMAD of the nanocomposite particles are comparable to the values of the blank carrier particles suggesting that the aerosolization is largely dictated by the carrier particles. Despite their larger $d_{A,theory}$ – 6.4 μm versus 5.2 μm for $R_{Nanoparticle/carrier} = 0.83$ and 0.53, respectively – FPF of the nanocomposite particles produced at $R_{Nanoparticle/carrier} = 0.83$ is slightly higher (i.e. ≈24 ± 2% with MMAD = 3.4 μm) than

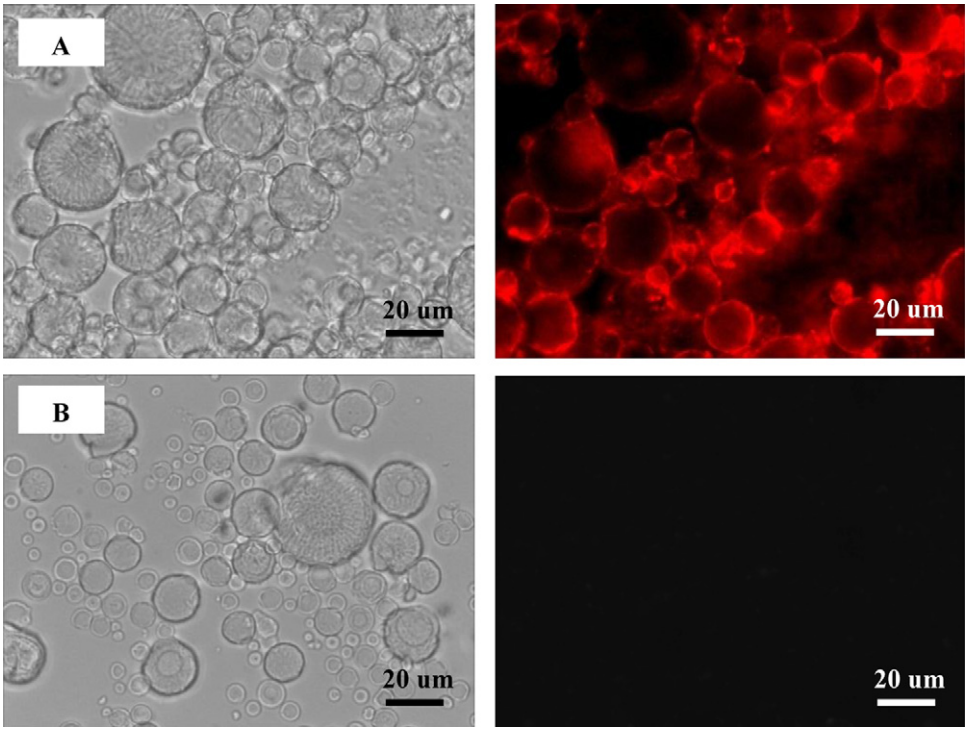

Fig. 3. (A) Successful adsorption of the cationic PLGA–PC/SA nanoparticles onto the anionic CS/TPP/DXT carrier particles ($R_{Nanoparticle/carrier} = 0.83$), (B) but not for the anionic PLGA–PC nanoparticles ($R_{Nanoparticle/carrier} = 0.53$).

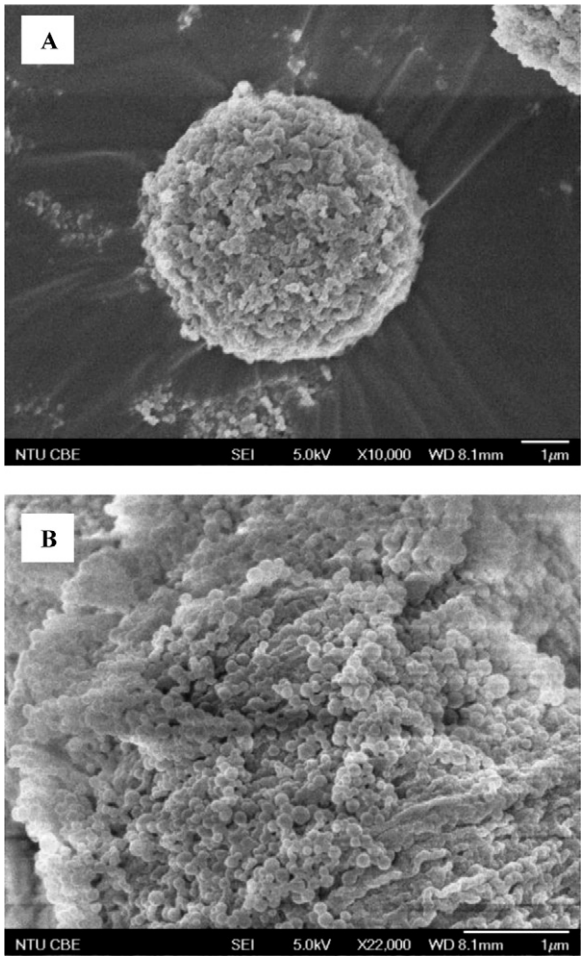

Fig. 4. FE-SEM images of (A) microscale nanocomposite of cationic PLGA–PC/SA nanoparticles and (B) a close-up view shows good coverage of the carrier particle surface by the nanoparticles.

those produced at $R_{\text{Nanoparticle/carrier}} = 0.53$ (i.e. FPF = 17 ± 2% and MMAD = 5.6 μm). Both products nevertheless possess similar ED at ≈75%. A closer look at the deposition patterns of the two products in Fig. 8 indicates nearly identical patterns up to stage 1. Variations

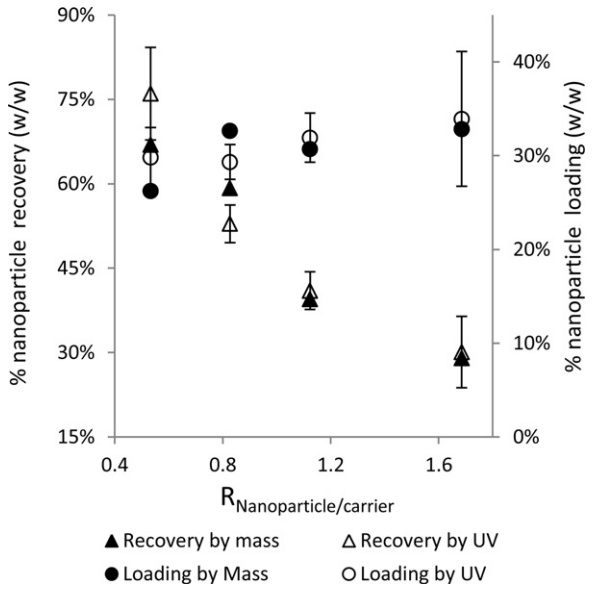

Fig. 6. Agreement between % nanoparticle recovery and % loading obtained by mass and UV–Vis measurements.

in the deposition patterns of the two products are mainly observed in stages 2–5.

5. Discussion

5.1. Inhalable carrier particles

We prepare carrier particles with $d_{G,dry}$ in the order of ≈10 μm because particles of a smaller order of magnitude (e.g. 1 μm) are difficult to aerosolize due to their significant surface force interaction, whereas particles of a larger order of magnitude (e.g. 100 μm) require extremely low ρ_e (<0.1 g/cm^3) to obtain $1 \le d_{A,theory} \le 5$ μm, rendering them highly fragile. For the 10 μm carrier particles to exhibit $1 \le d_{A,theory} \le 5$ μm, they must exhibit degree of porosity in the range of $\rho_e \approx 0.3$ g/cm^3 according to Eq. (1). CS particles prepared by ionic cross-linking are used as they are known to exhibit high degree of porosity (Agnihotri et al., 2004). Nevertheless, the porous CS particles must also be sufficiently robust to endure the drying process and aerosolization forces.

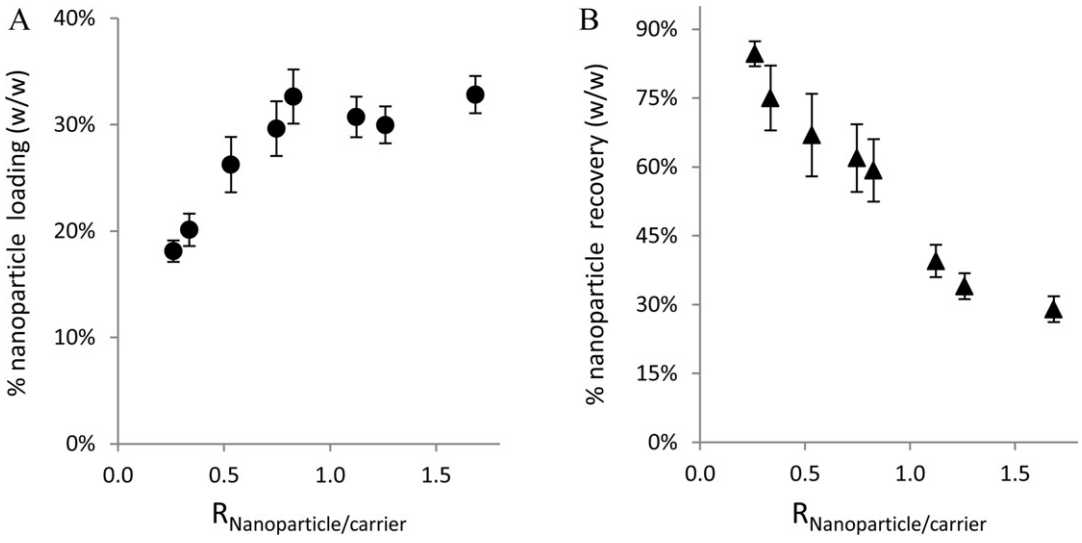

Fig. 5. (A) % nanoparticle loading and (B) % nanoparticle recovery as a function of $R_{\text{Nanoparticle/carrier}}$.

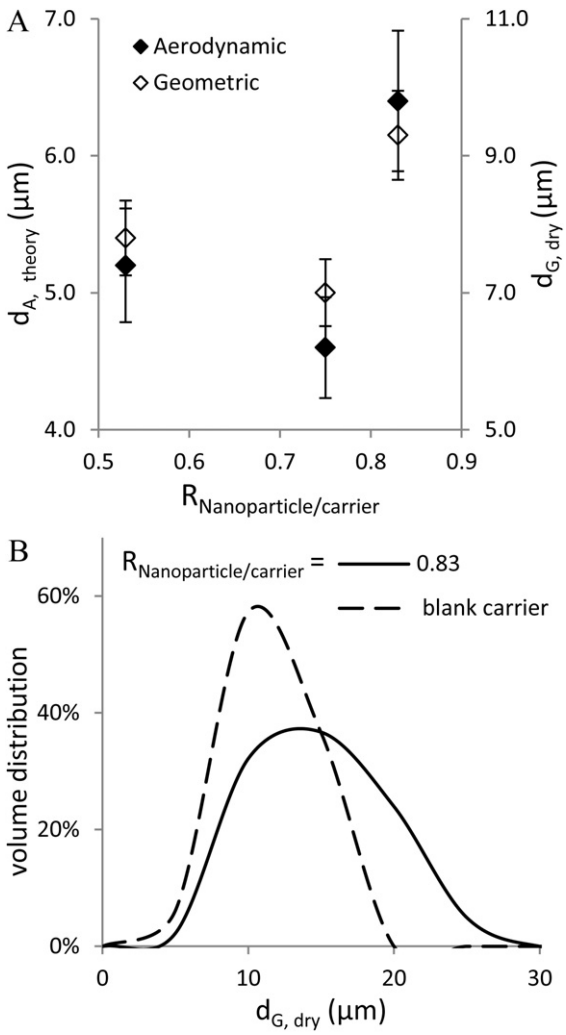

Fig. 7. (A) $d_{A,theory}$ and $d_{G,dry}$ of the nanocomposite particles as a function of $R_{Nanoparticle/carrier}$, and (B) $d_{G,dry}$ distribution of the nanocomposite particles compared to the blank carrier particles.

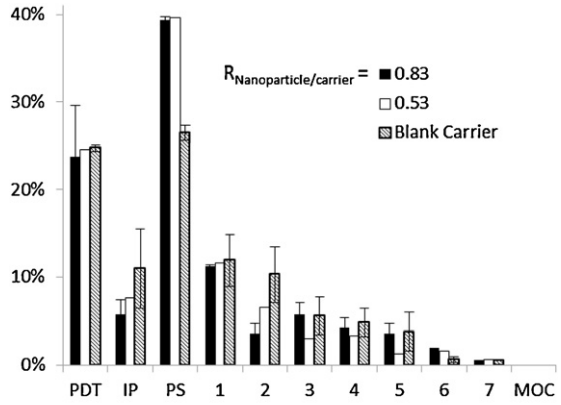

$R_{Nanoparticle/carrier}$	ED (w/w)	FPF (w/w)	MMAD (μm)
0.0	75 ± 1	27 ± 7	4.9 ± 0.8
0.53	75 ± 6	17 ± 2	5.6 ± 1.5
0.83	76 ± 6	24 ± 2	3.4 ± 0.9

Fig. 8. Aerosolization characteristics of the nanocomposite particles.

The use of atomization to prepare ionically cross-linked CS particles having a certain size range was pioneered by (Albertini et al., 2005), where using an ultrasonic atomizer, they produced CS particles having $d_{G,dry}$ = 50–200 μm, which was significantly smaller than >500 μm particles produced by using syringe or spray guns. To have a definite control over the particle size, they performed the CS crosslinking at excess charge of the crosslinker (i.e. TPP), whereby the CS droplet, upon hitting the crosslinking solution, was immediately crosslinked and transformed into rigid particles. Consequently, the resultant particle size was dictated by the CS droplet size, which could be manipulated with great certainties by adjusting the atomization parameters.

Following (Albertini et al., 2005), we carry out the crosslinking at a minimum of seven times excess TPP charge resulting in the formation of spherical CS particles with $d_{G,wet} \approx 10–30$ μm. A two-fluid atomizer is used in place of an ultrasonic one as the two-fluid atomizer enables production of droplets with diameters < 50 μm. Without the excess TPP charge, our study indicates that the resultant particle size becomes less predictable as it is influenced by myriad of parameters (e.g. stirring rate, aging time, pH) (data not shown). For the CS concentration investigated (i.e. 1.0%, w/v), $d_{G,wet} \approx 10–30$ μm translates to carrier particles having $d_{G,dry}$ (≈7–9 μm) and ρ_e (≈0.5 g/cm^3).

At lower TPP excess charge ratios, loose agglomerates of CS droplet-turn-particles are formed on the surface of the crosslinking solution. The lower TPP concentration (i.e. TPP/CS mass ratio < 2.5) slows down the CS droplet crosslinking resulting in the formation of soft and non-spherical CS particles due to the lack of crosslinked CS molecules in the periphery. These particles are prone to agglomeration with the neighbouring CS particles due to their lack of rigidity. Similarly, the agglomeration observed for particles prepared at a lower CS concentration (i.e. 0.5%, w/v) is attributed to the slower droplet crosslinking in the periphery resulting in the same lack of rigidity. The use of the two-fluid atomizer is crucial in this regard as the high-speed airflow enhances the mixing between the CS droplet and the crosslinking solution, therefore ensuring fast crosslinking in the CS droplet periphery, resulting in the production of rigid, spherical, and well dispersed CS particles.

Despite their sound structural integrity in the wet state, the CS/TPP particles produced in Run 1 are unable to withstand the freezing and drying stresses generated in the freeze drying process (i.e. ice crystal formation and sublimation), causing them to collapse and aggregate after freeze drying. Oven drying of the particles also results in the aggregation. To solve the aggregation problem, we try extending the aging time of the crosslinked particles from 1 to 4 h aimed to increase the crosslinking density, hence improving particle robustness. The aggregation after drying, however, persists. The particle robustness can certainly be improved by increasing CS concentration, or by hardening the CS droplet, via coacervation in alkaline solutions or coagulation with gelatin, prior to crosslinking. However, these approaches would produce CS/TPP particles having higher ρ_e resulting in $d_{A,theory} > 5$ μm.

Adding polyionic macromolecules, such as alginate and DXT, to improve the robustness of CS/TPP particles has been attempted before (Lin et al., 2005; Shu and Zhu, 2000). These studies, however, were conducted at a much larger particle length scale in the order of several hundred microns. To investigate how DXT can improve the robustness of CS/TPP particles, we carry out a trial experiment using a syringe to prepare large CS/TPP/DXT particles, whose internal structures can be examined by FE-SEM. Without DXT, porous CS/TPP particles are produced after freeze drying (Fig. 9A). Whereas in the presence of DXT, a thick layer of material, which is likely made up of DXT, is formed in the exterior of the CS/TPP particles signifying the core–shell nature of the CS/TPP/DXT particles (Fig. 9B). The envelopment of the porous CS/TPP core by the solid DXT shell translates to their higher structural integrity. The

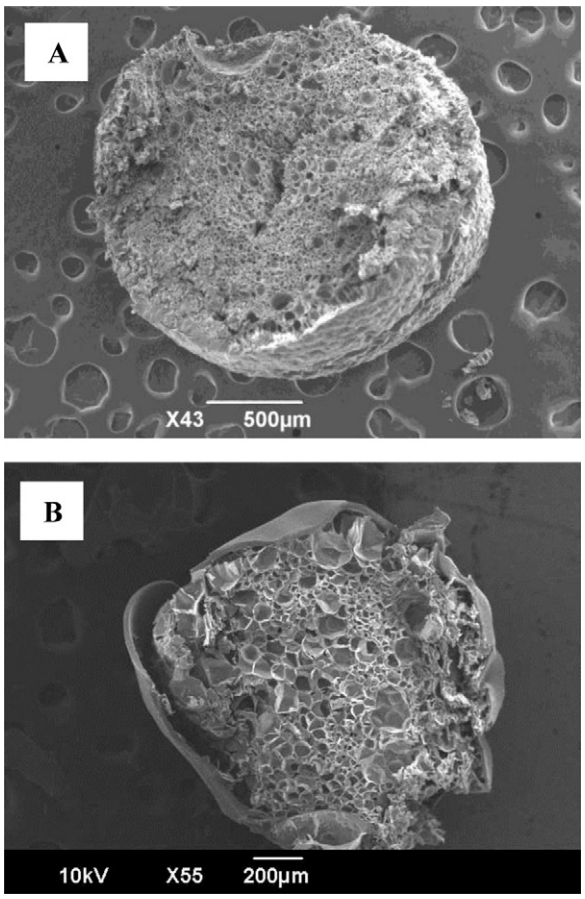

Fig. 9. (A) CS/TPP at CS:TPP = 2.0:2.5% (w/v), (B) CS/TPP/DXT at CS:TPP:DXT = 2.0:2.5:2.5% (w/v).

core–shell structure is also observed in the smaller CS/TPP/DXT particles produced by atomization as manifested by the high surface asperities not observed in the CS/TPP particles.

The role of DXT in providing mechanical stabilization of the CS/TPP particles enables us to operate at low CS concentrations crucial in maintaining low ρ_e. Furthermore, with DXT inclusion, a lower degree of excess TPP charge is needed to produce rigid, spherical, and well dispersed particles, which is manifested by a successful particle production in Run 2 at CS:TPP = 1.0:1.0% (w/v). CS crosslinking with DXT in the CS droplet periphery is believed to contribute to additional mechanical stability, such that less TPP is needed. Having too low TPP concentration, such as 0.5% (w/v) in Run 3, however, leads to very slow crosslinking by TPP, which likely opens up a window for the large molecule DXT to crosslink with CS in the core as well, resulting in the formation of denser particles, which do not shrink as much after drying, hence larger $d_{G,dry}$. To confirm that the CS crosslinking at 0.5% (w/v) TPP is slow, an experiment at TPP concentration of 0.5% (w/v), without any DXT, is performed. The particle formation is observed visually to occur more slowly than the instantaneous particle formation at 1.0% (w/v) TPP, hence corroborating the lower crosslinking rate at 0.5% (w/v) TPP. Using DXT as the primary crosslinking agent (i.e. without TPP), however, produces highly fragile particles, even in their wet state, where the particles formed are observed to be prone to breakage even by coming into contact with the stirrer bar.

5.2. Hybrid nanoparticle adsorption and desorption

The presence of DXT shell in the CS/TPP/DXT particles makes their surface highly negatively charged, such that only the cationic hybrid nanoparticles can be adsorbed. In contrast, the CS/TPP carrier particles from Run 1, which are also negatively charged, but not as high due to the absence of DXT shell, can attract both cationic and anionic hybrid nanoparticles. The anionic nanoparticles are adsorbed onto the CS/TPP particles through their electrostatic interactions with exposed anionic CS molecules. Nonetheless, the extent of adsorption for the anionic nanoparticles onto the CS/TPP carrier particles is low with both % recovery and % loading around 10%. Even for the cationic nanoparticles, the % recovery and % loading for their adsorption onto the CS/TPP particles are substantially lower (i.e. ≈30% and 15%, respectively, at $R_{Nanoparticle/carrier} = 0.53$) compared to their adsorption onto the CS/TPP/DXT particles. Furthermore, the CS/TPP nanocomposite particles still form aggregates after drying even after having nanoparticles adsorbed on their surface. Therefore, the DXT inclusion is crucial not only in mechanical stabilization, but also in nanoparticle adsorption.

Significantly, the results of the adsorption onto CS/TPP particles suggest that the nanoparticle adsorption is not dictated solely by the net electrostatic charge of the carrier particles, but also is influenced by the individual charge of the components making up the carrier particles. As the ionically crosslinked carrier particles always have both cationic and anionic components, both cationic and anionic nanoparticles can be adsorbed onto carrier particles that are specifically engineered for this purpose. The immediate future research direction is therefore to develop universal carrier particles, which can attract both anionic and cationic hybrid nanoparticles at high efficiency, while are physically robust at the same time.

Even though the CS/TPP/DXT carrier particles readily attract the oppositely charged hybrid nanoparticles, the optimal % nanoparticle loading at ≈30% (w/w) for $0.53 \leq R_{Nanoparticle/carrier} \leq 0.83$ still leaves much room for improvement due to less than optimal nanoparticle adsorption. For comparison, putting their drawbacks aside (e.g. low yield, safety risks), the optimal DPI formulations of the same hybrid nanoparticles by SD and SFD in Wang et al. (2012) contain 50% (w/w) nanoparticle loading, with the rests being the drying adjuvants. Nevertheless, the optimal % nanoparticle recovery at ≈65% obtained in the present technique represents a significant improvement over the nanoparticle recovery in SD, while is comparable to the value in SFD (Wang et al., 2012). The optimal % recovery could have been higher if the nanoparticle adsorption is more efficient.

Increasing $R_{Nanoparticle/carrier}$ high above unity does not lead to higher % loading, instead only lower % recovery, suggesting that the low % loading is not due to the lack of nanoparticles. The low % loading is not due to the lack of surface for adsorption either as the FE-SEM image of the nanocomposite particles in Fig. 4B indicates that the carrier particle surface is not yet fully occupied by the nanoparticles. One plausible explanation for the low % loading is that the PLGA–PC/SA nanoparticles that are already adsorbed onto the carrier particles, upon reaching a certain critical mass, begin to exert repulsive electrostatic forces to their surroundings, which deters adsorption of the remaining free nanoparticles. The critical mass is likely reached at the current plateau of the % loading (≈30%).

To circumvent this problem, the nanoparticle adsorption can be performed in stages with increasing presence of salt towards later stages. The presence of salt in the second stage would screen the repulsive electrostatic forces generated by the already adsorbed nanoparticles from the first stage, hence facilitating adsorption of the remaining nanoparticles in the second stage, and so on. The charge screening role of salt has been demonstrated in layer-by-layer coating of surfaces by oppositely charged polyelectrolytes, where higher salt concentrations result in thicker coatings as more polyelectrolyte molecules are attracted to the oppositely charged surfaces (Dahlgren et al., 1993). In our preliminary experiment using 0.1 M NaCl solution, however, the effect of salt inclusion

on the nanoparticle adsorption is found to be minimal suggesting that the current repulsive electrostatic forces, generated by the nanoparticles already adsorbed on the carrier particles, are strong enough to overcome the charge screening effect of the salt. Therefore, future experiments must be conducted at higher salt concentrations.

Once the nanoparticles are successfully adsorbed onto the CS/TPP/DXT carrier particles, the strong electrostatic interaction between them, attributed to the high charge density of the carrier particles, leads to difficult nanoparticle desorption. Furthermore, the hydrophobicity of the hybrid nanoparticles used in the present experiments may have contributed to poor wettability, hence the less than optimal desorption of the nanoparticles. The ineffective nanoparticle desorption would jeopardize their therapeutic effectiveness as the nanoparticles become vulnerable to lung phagocytic clearances and their targeting ability is diminished. The nanoparticle desorption can certainly be improved in the laboratory setting by having intense agitations of the powder suspension. However, this approach is not pursued as it does not represent a realistic environment of the intended application. In this regard, instead of investigating the effect of carrier charge density on the nanoparticle desorption, whose findings are likely applicable to only one nanoparticle type, the future research direction should develop carrier particles that quickly disintegrate due to intense swelling in PBS, thereby releasing the nanoparticles. Such carrier particles would be applicable to a large number of nanoparticles.

5.3. Physical and aerosolization characteristics

Despite their similar % nanoparticle loading and the same carrier particles are used, $d_{G,dry}$ of the nanocomposite particles produced at different $R_{Nanoparticle/carrier}$ exhibit some variations, albeit not very significant ($\pm 2\,\mu m$). The $d_{G,dry}$ variations are likely caused by an unequal amount of adsorbed nanoparticles per carrier particle, as a result of the difference in the amount of nanoparticles present. The $d_{G,dry}$ variations make the aerosolization efficiency dependent on $R_{Nanoparticle/carrier}$, where the optimal FPF and MMAD are exhibited by the nanocomposite particles produced at $R_{Nanoparticle/carrier} = 0.83$, which possess the largest $d_{G,dry}$. This is despite their $d_{A,theory}$ being larger than 5 μm, which is worse than the particles produced at $R_{Nanoparticle/carrier} = 0.53$ ($d_{A,theory} \approx 5\,\mu m$). This observation, however, is not uncommon as $d_{A,theory}$ does not take into account particle agglomeration upon aerosolization, which influences particle deposition patterns in the NGI. The slight variations in the FPF and MMAD between the particles produced at $R_{Nanoparticle/carrier} = 0.53$ and 0.83 are believed to be caused by the difference in their agglomeration tendency, rather than the difference in their individual particle characteristics.

The optimal ED, FPF, and MMAD of the nanocomposite particles produced by the present technique are comparable to the values obtained from SD and SFD (Wang et al., 2012). The lower % loading in the present nanocomposite particles, however, translates to fewer nanoparticles being delivered to the lung. As the aerosolization efficiency (i.e. ED, FPF, and MMAD) of the nanocomposite particles largely depends on the characteristics of the carrier particles, nanocomposite particles with higher % loading are expected to exhibit aerosolization efficiency of similar magnitude.

With respect to the commercial DPI formulations, which use coarse lactose particles to facilitate aerosolization of the drug particles, the amount of nanoparticles delivered to the lung by the present formulation is also comparable. For 10 mg dose, at ED ≈ 75%, FPF ≈ 25%, and % loading ≈ 30%, the nanocomposite particles would deliver ≈0.56 mg of nanoparticles ($0.75 \times 0.25 \times 0.30 \times 10$ mg). For the commercial DPI formulations, the coarse lactose fraction is typically at ≈80–99%, which translates to % loading of ≈1–20% (Srichana et al., 1998; Steckel and Muller, 1997). ED and FPF of commercial DPI formulations are on average ≈ 70–80% and ≈20–30%, respectively (Donovan and Smyth, 2010), resulting in a maximum of ≈0.54 mg drug particles delivered for 10 mg dose.

6. Conclusion

We have successfully developed a new DPI formulation technique of lipid–polymer hybrid nanoparticles in the form spherical nanocomposite particles, by means of electrostatically-driven assembly of the nanoparticles on oppositely-charged polysaccharide carrier particles. Our new technique exhibit advantages over the conventional techniques in terms of its nanoparticle recovery, scalability, batch-to-batch consistency, ease-of-preparation, cost, and applicability to different nanoparticles with only minimal modifications required. The challenge of preparing inhalable CS carrier particles, which are physically robust at the same time, has been solved by having DXT as CS crosslinker, in addition to TPP, resulting in the formation of particles with a core–shell structure. The optimal nanoparticle to carrier mass ratio that produces the best combination of % nanoparticle loading and % recovery has been determined.

The carrier particle characteristics largely dictate the aerosolization efficiency of the nanocomposite particles with minimal, but not negligible influence, from the nanocomposite particle characteristics themselves. The present nanocomposite particles exhibit aerosolization efficiency that is comparable to that obtained from existing DPI formulations. The present formulation, however, still leaves much room for improvement due to the relatively low nanoparticle loading and ineffective nanoparticle desorption. Feasible solutions to improve the nanoparticle loading and desorption efficiency have been proposed. Lastly, the present CS/TPP/DXT carrier particles are limited to adsorption of cationic nanoparticles due to their highly negatively charges. Therefore, the immediate future research direction is to prepare carrier particles that are more universal in a sense that they can attract both cationic and anionic hybrid nanoparticles at equally high efficiency.

Acknowledgement

The authors gratefully acknowledge the funding from Ministry of Education of Singapore AcRF Tier I Fund (Grant No. RG 76/10).

Appendix A. Supplementary data

Supplementary data associated with this article can be found, in the online version, at http://dx.doi.org/10.1016/j.ijpharm.2012.05.036.

References

Agnihotri, S.A., Mallikarjuna, N.N., Aminabhavi, T.M., 2004. Recent advances on chitosan-based micro- and nanoparticles in drug delivery. J. Control. Release 100, 5–28.

Albertini, B., Passerini, N., Rodriguez, L., 2005. Evaluation of ultrasonic atomization as a new approach to prepare ionically cross-linked chitosan microparticles. J. Pharm. Pharmacol. 57, 821–829.

Bhumkar, D.R., Pokharkar, V.B., 2006. Studies on effect of pH on cross-linking of chitosan with sodium tripolyphosphate: a technical note. AAPS PharmSciTech, 7.

Dahlgren, M.A.G., Waltermo, A., Blomberg, E., Claesson, P.M., Sjoestroem, L., Aakesson, T., Joensson, B., 1993. Salt effects on the interaction between adsorbed cationic polyelectrolyte layers: theory and experiment. J. Phys. Chem. 97, 11769–11775.

Donovan, M.J., Smyth, H.D.C., 2010. Influence of size and surface roughness of large lactose carrier particles in dry powder inhaler formulations. Int. J. Pharm. 402, 1–9.

Edwards, D.A., 2002. Delivery of biological agents by aerosols. AlChE J. 48, 2–6.

El-Gendy, N., Berkland, C., 2009. Combination chemotherapeutic dry powder aerosols via controlled nanoparticle agglomeration. Pharm. Res. 26, 1752–1763.

Kam, S.K., Gregory, J., 1999. Charge determination of synthetic cationic polyelectrolytes by colloid titration. Colloid Surface A 159, 165–179.
Kho, K., Cheow, W.S., Lie, R.H., Hadinoto, K., 2010. Aqueous re-dispersibility of spray-dried antibiotic-loaded polycaprolactone nanoparticle aggregates for inhaled anti-biofilm therapy. Powder Technol. 203, 432–439.
Lin, W.-C., Yu, D.-G., Yang, M.-C., 2005. pH-sensitive polyelectrolyte complex gel microspheres composed of chitosan/sodium tripolyphosphate/dextran sulfate: swelling kinetics and drug delivery properties. Colloid Surface B 44, 143–151.
Schiffter, H., Condliffe, J., Vonhoff, S., 2010. Spray-freeze-drying of nanosuspensions: the manufacture of insulin particles for needle-free ballistic powder delivery. J. R. Soc. Interface 7, S483–S500.
Shi, L.J., Plumley, C.J., Berkland, C., 2007. Biodegradable nanoparticle flocculates for dry powder aerosol formulation. Langmuir 23, 10897–10901.
Shu, X., Zhu, K.J., 2000. A novel approach to prepare tripolyphosphate/chitosan complex beads for controlled release drug delivery. Int. J. Pharm. 201, 51–58.
Srichana, T., Martin, G.P., Marriott, C., 1998. Dry powder inhalers: the influence of device resistance and powder formulation on drug and lactose deposition in vitro. Eur. J. Pharm. Sci. 7, 73–80.
Steckel, H., Muller, B.W., 1997. In vitro evaluation of dry powder inhalers. 2. Influence of carrier particle size and concentration on in vitro deposition. Int. J. Pharm. 154, 31–37.
Su, X.F., Fricke, J., Kavanagh, D.G., Irvine, D.J., 2011. In vitro and in vivo mrna delivery using lipid-enveloped pH-responsive polymer nanoparticles. Mol. Pharm. 8, 774–787.
Sung, J., Padilla, D., Garcia-Contreras, L., VerBerkmoes, J., Durbin, D., Peloquin, C., Elbert, K., Hickey, A., Edwards, D., 2009. Formulation and pharmacokinetics of self-assembled rifampicin nanoparticle systems for pulmonary delivery. Pharm. Res. 26, 1847–1855.
Sung, J.C., Pulliam, B.L., Edwards, D.A., 2007. Nanoparticles for drug delivery to the lungs. Trends Biotechnol. 25, 563–570.
Wang, Y.J., Kho, K., Cheow, W.S., Hadinoto, K., 2012. A comparison between spray drying and spray freeze drying for dry powder inhaler formulation of drug-loaded lipid–polymer hybrid nanoparticles. Int. J. Pharm. 424, 98–106.
Zhang, L., Chan, J.M., Gu, F.X., Rhee, J.-W., Wang, A.Z., Radovic-Moreno, A.F., Alexis, F., Langer, R., Farokhzad, O.C., 2008. Self-assembled lipid–polymer hybrid nanoparticles: a robust drug delivery platform. ACS Nano 2, 1696–1702.